ACS APPLIED POLYMER MATERIALS

pubs.acs.org/acsapm Article

Investigating Correlations in Hydroxide Ion Transport in Anion Exchange Membranes from Atomistic Molecular Dynamics Simulations

Mohammed Al Otmi, Ping Lin, William Schertzer, Coray M. Colina, Rampi Ramprasad, and Janani Sampath*

Cite This: ACS Appl. Polym. Mater. 2024, 6, 11270−11279 Read Online

ACCESS | Metrics & More | Article Recommendations | Supporting Information

ABSTRACT: Anion exchange membranes offer a promising alternative to the more expensive proton exchange membrane fuel cells; however, hydroxide ion conductivity in anion exchange membranes is poorly understood. In this paper, we use classical molecular dynamics simulations to study the structure and ion transport properties of four different polyethylene-based membranes prepared from ethylene-*co*-vinyl-acetate (EVA). We examine the microstructure of the membranes and find that polymers with a narrow cavity size distribution have tighter packing of water molecules around hydroxide ions, compared to membranes with a broad cavity distribution. We calculate the structure factor of the hydrated membranes and find a peak between 1 and 4 nm^{-1}, characteristic of ionic clusters in these materials. We estimate the self-diffusion coefficient of water and hydroxide ions and find that water molecules have a higher diffusion than hydroxide ions across all systems. The trends in hydroxide diffusion align well with experimental conductivity measurements. For systems with broad cavities, water facilitates hydroxide diffusion through vehicular transport, and in systems with narrow cavities, both ion hopping and vehicular transport are observed; this is quantified by calculating ion−ion and ion−solvent correlations through the Onsager transport coefficient framework.

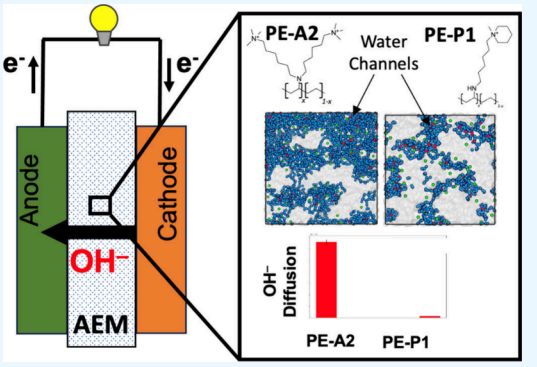

KEYWORDS: *Polymer membranes, Ion exchange, Molecular dynamics simulations, Hydroxide transport, Ionomers*

INTRODUCTION

Polymer anion exchange membranes (AEMs) which contain a positively charged functional group and facilitate the transport of hydroxide anions are widely studied, as they are used in alkaline fuel cells. AEMs offer a less expensive alternative to proton exchange membranes (PEMs) such as Nafion which have been extensively used due to their stability, processability, and high conductivity.[1] While PEM fuel cells exhibit excellent performance, their reliance on costly catalysts, notably platinum, has posed economic challenges.[2] In contrast, alkaline fuel cells have faster reaction kinetics, which facilitate the utilization of less expensive catalysts.[3] This has sparked considerable interest in both academic and industrial sectors toward identifying optimal AEMs to be used in alkaline fuel cells.

While AEMs demonstrate remarkable energy conversion efficiency, the quest for an AEM material with superior ion conductivity, robust mechanical properties, and high chemical stability is ongoing.[4] The diffusion of hydroxide ions (OH^-) in AEMs is four times slower compared to the diffusion of protons (H^+) in PEMs. To achieve conductivity comparable to PEMs, a higher ion exchange capacity (IEC) is required.[5] However, a high IEC usually leads to considerable swelling of the membrane, which compromises the mechanical robustness of the membrane module.[6] Furthermore, quaternary ammonium functional groups, which constitute the polymer cations in many AEMs, undergo nucleophilic attack by hydroxide ions leading to membrane degradation.[7] Several studies have focused on modifying the side chain of the quaternary ammonium functional group to improve both conductivity and chemical and mechanical stability.[8−10]

To enhance conductivity without compromising mechanical and chemical stability, we need a clear understanding of hydroxide ion transport through the polymer matrix. Key contributors to ion transport include morphology of polymer membranes and water uptake. These factors also control the mechanical integrity of the membrane, making it imperative to

Received: June 14, 2024
Revised: September 3, 2024
Accepted: September 3, 2024
Published: September 12, 2024

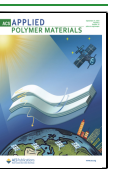

study the morphology (or microstructure) of the polymer as a function of water uptake to improve emergent properties, such as ion transport and membrane strength. When hydrated, cavities in the polymer matrix undergo swelling resulting in the creation of continuous water channels that facilitate both vehicular and Grotthuss (proton hopping) diffusion of hydroxide ions.[11] At low hydration levels, hydroxide ions neutralize the cationic sites, degrading the membrane.[12] Therefore, moderate to high hydration levels are maintained in AEMs, and ion transport is mediated primarily by water.[13,14] Even then, OH^- dynamics are challenging to characterize as the motion of the hydroxide ions is coupled with the polymer backbone, water molecules, as well as other OH^- ions. A recent study used quasi-elastic neutron scattering (QENS) to decouple water and polymer relaxation dynamics from the diffusional dynamics of hydroxide ions.[15] The authors suggest that the diminished efficiency of anion transport at lower hydration levels arises from the lack of coupling with water diffusional dynamics. Water molecules are needed to facilitate OH^- transport, and a molecular-level understanding of the OH^- and water transport mechanisms within AEMs is critical for optimizing their performance and efficiency.

Molecular dynamics (MD) simulations can provide important insights into the molecular level interactions and the transport mechanism of hydroxide ions in AEMs. By employing detailed ab initio calculations, Zelovich et al. demonstrated that OH^- ions attract a cluster of water molecules, with the number of molecules in each cluster ranging from one to five, depending on the hydration level.[16] The first solvation shell forms at a distance of 3.7 Å from the OH^- ion, encompassing 1−3 water molecules depending on the hydration number. In bulk solution, the first hydration shell around OH^- comprises four water molecules.[16−18] ReaxFF molecular dynamics simulations used radial distribution function to show that the first hydration shell contains 3.5 and 4.2 water molecules in low and high hydration levels, respectively.[19] The contribution of vehicular and Grotthuss diffusion is dependent on the hydration number (λ); at $\lambda = 4$ or lower, water mediated OH^- hopping (Grotthuss) is the dominant mechanism.[13,15] A study by Chen et al. also showed that a combination of both vehicular and Grotthuss diffusion contributes to the overall transport, but they emphasized that vehicular diffusion is significantly more dominant at hydration levels of $\lambda > 14$.[20] Zhang and van Duin investigated three functionalized poly(phenylene oxide) polymers using both classical and reactive force fields. The study examined the effect of water content and showed that OH^- diffusion increases with the increase in the hydration level. They also found that increasing the alkyl chain length on the cationic side of quaternary ammonium protects N^+ from nucleophilic attack.[19] Another study delved into the OH^- transport mechanism using a polarizable force field and highlighted the effect of bottlenecks formed in the polymer matrix.[5] The study shows that the formation of narrow regions (bottlenecks) influences the water channels and has an adverse effect on ion transport. Transport through these narrow bottlenecks via vehicular diffusion is thermodynamically unfavorable as it requires the hydroxide ion to partially dehydrate first leading to a significantly higher contribution from Grotthuss transport. Limiting the number of bottlenecks and achieving a desirable water channel morphology can lower the energy barrier for hydroxide transport through vehicular diffusion.[5] Other studies using both classical and reactive force fields have shown that the Grotthuss diffusion dominates in confined environments and have highlighted the importance of Grotthuss hopping when dealing with subnanometer wide water channels.[21,22]

In this study, we focus on how polymer morphology affects OH^- transport and mechanical properties, in polyethylene based AEMs by employing classical molecular dynamics (MD) simulations. We systematically analyze four systems that have been characterized experimentally and offer molecular insights into experimentally observed trends by relating ion dynamics to polymer morphology and chemistry. These systems have the same backbone structure, which allows us to correlate functional group chemistry to overall performance. We assess vehicular transport and its relationship to polymer microstructure, to understand the underlying dynamics and mechanisms involved. We calculate ion−ion correlations and offer insights into how different side chain groups affect hydroxide transport. Understanding how ions move in the polymer matrix and how water channels and the structure of the polymer influence ion transport is crucial for optimizing AEM design and enhancing their properties. We expect that these insights can guide the design of new AEMs with enhanced OH^- dynamics and mechanical properties.

MATERIALS AND METHODS

System Setup. Four AEM chemistries featuring similar backbone chains are selected to investigate how side chain architecture impacts the performance of AEMs (Figure 1). Specifically, the chosen

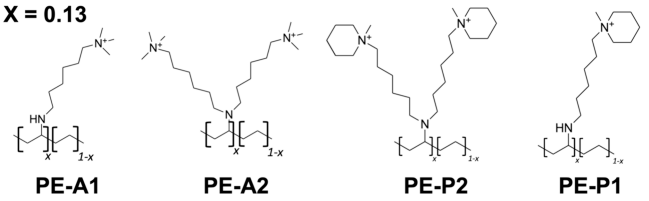

Figure 1. Anion exchange membrane chemistries investigated in this study. Four ammonium-functionalized polyethylene are divided depending on the functional groups.

polymers are ammonium-functionalized polyethylene (PE-F) that contain two different cationic functional groups, with different alkyl chain branching, as detailed in the study by Wang et al.[23] For simplicity, we will use the abbreviations PE-F, where F denotes a specific functional group, to refer to these systems. These abbreviations which we will use throughout the manuscript correspond to the functionalized polymers depicted in Figure 1.

We vary the number of alkyl chains attached to the polymer backbone (1 or 2), as well as the type of functional group at the end of the alkyl chains. The alkyl chain length is constant, with 6 $-CH_2$ groups. The backbone is 13% functionalized with either trimethylammonium (TMA) or *N*-methylpiperidinium (NMP) groups. These particular compositions are selected based on their superior performance, as documented in the study by Wang et al.[23] Systems are referred to as PE-A1 and PE-A2 if they are functionalized with 1 or 2 TMA groups, respectively, and PE-P1 and PE-P2, if they contain 1 or 2 NMP groups, respectively. The four chemistries are chosen for their systematic changes in polymer architecture and total ion content.

Monomer units are constructed using Avogadro,[24] followed by geometry optimization using the semiempirical GFN2-xTB method.[25] The assignment of the force field parameters is carried out using Antechamber.[26] Both atom types and force field parameters are determined in accordance with the General Amber Force Field (GAFF2).[27] The AM1-BCC method is used to assign atomic partial charges.[28] Explicit water molecules are inserted, and their interactions are represented using a flexible SPC/E water model.[29] Subsequently,

https://doi.org/10.1021/acsapm.4c01827
ACS Appl. Polym. Mater. 2024, 6, 11270−11279

Pysimm[30] is employed to generate various polymer chains using the random walk simulated polymerization algorithm. Ions and water molecules are incorporated into the system using Packmol.[31] The number of OH^- ions is varied to investigate different ion exchange capacities, while adjustments are made to hydration levels to replicate the reported experimental water uptake. In all systems, water plays a crucial role in enhancing ion conductivity, necessitating an adequate water uptake to establish interconnected hydrated domains that facilitate ion diffusion.[32−35] In our simulations, we used the reported water uptake values to calculate the hydration number as defined in eq 1. Here, the hydration number (λ) is determined using the theoretical ion exchange capacity (IEC, mmol[OH]/g), the molecular weight of water (M_{wt}, g/mol), the experimental water uptake (WU% H_2O), and a constant 10 for unit adjustment. Theoretical IEC is determined from the elemental analysis of the dry AEM composition. Four independent replica simulations with different starting configurations (which includes independent monomer packing and polymerization) are carried out for each of the four systems described above, for a total of 16 systems. The system parameters are listed in Table S1.

$$\lambda = \frac{\text{WU\% } H_2O \times 10}{\text{IEC} \times M_{wt}} \tag{1}$$

After the replicas are constructed, we employ a 21-step annealing protocol[36] to achieve system equilibration, during which each replica is allowed to relax to its equilibrium density. Then all replicas undergo an additional 1 ns run in the NVT ensemble, at a temperature of 300 K. Following this, the replicas continue to run in the same ensemble for 20 ns (hydroxide ions and water molecules attain diffusive behavior over this period), during which data are collected. Data shown are the average over the four replicas for each system. All simulations in this work are run using Large Scale Atomic Massively Parallel Simulator (LAMMPS).[37] Nosé−Hoover thermostat with a damping factor of 100 ps is used in the equilibration and production simulations, and Nosé−Hoover barostat is coupled to the thermostat with a pressure damping parameter of 100 ps during the 21-step annealing process. A velocity-verlet integrator with a 1 fs time step is employed. Long ranged interactions are accounted for by employing a particle−particle/particle-mesh (PPPM) algorithm with a 1.5 nm cutoff.

Analysis. To assess water channels across the different hydrated polymer samples, we examine the channel dimensions, or voids within the polymer matrix. This entails removal of ions and water molecules from different samples and characterizing unoccupied regions of the polymer matrix (which would be occupied by ions and water in the hydrated polymer). To accomplish this, we take a fully saturated membrane at the end of the 20 ns run, remove all ions and water molecules from this membrane, and quantify the voids which are left behind in place of the water molecules and ions. Then, we apply Void Analysis Codes and Unix Utilities for Molecular Modeling and Simulations, or VACUUMMS.[38,39] VACUUMMS is an open-source software package that leverages the Cavity Energetic Sizing Algorithm (CESA),[40] which is a Monte Carlo-based energetic technique employed to characterize voids within a polymer matrix. In the CESA method, cavities are defined as spherical volumes with energy centers, which correspond to local minima in the repulsive energy field of the particles. This approach allows for the determination of a size distribution of voids, collectively constituting the hydration channels within the material. We have used this method in the past to quantify voids in gas separation membranes.[41]

To evaluate the long-range order of the ions in the material, we compute the ion−ion structure factor. Mathematically, it is defined as

$$S_{N-OH}(k) = \frac{1}{N}\sum_{i=1}^{N}\sum_{j=1}^{N}\langle e^{-ik(r_i - r_j)}\rangle \tag{2}$$

where k is the wave vector, N is the number of ions, r_i is the position vector of the ith atom, r_j is the position vector of the jth atom. The wave vector k is discretized based on the size of the simulation box. We average this over the last frame of each of the four replicas.

To quantify the local packing of hydroxide ions near water molecules and the polymer cation, we utilize the radial distribution function (RDF), $g_{ij}(r)$, which is the normalized probability of an atom of type i existing at a distance r from an atom of type j. Specifically, we calculate $g_{H^*-H}(r)$, $g_{O^*-O}(r)$, $g_{O^*-N}(r)$, and $g_{N-N}(r)$, where H* and O* are the hydroxide hydrogen and oxygen, and H and O are water hydrogen and oxygen, respectively, and N is the nitrogen cation on the polymer backbone. We use the radial pair distribution function extension in VMD to compute $g_{ij}(r)$, and we average over the 20 ns runs of all replicas to compute each RDF.

To capture the dynamics of the hydroxide ions, water molecules, and polymer chains, we compute the mean squared displacement (MSD) for each species, given by

$$\text{MSD}(t) = <(r_i(t) - r_i(0))^2> \tag{3}$$

Here, $r_i(0)$ refers to the trajectory after 1 ns, and we do not perform any block averaging. Each MSD curve is averaged over four independent replicas. For each component (polymer chains, hydroxide ions, water), we compute MSD and plot it against time in a logarithmic scale. Polymer MSD is averaged over all atoms of the polymer. Once the MSD of OH^- and water attain diffusive behavior in each system (characterized by long time MSD slope $\approx$ 1), the diffusion coefficient can be calculated using Einstein's equation:

$$\text{MSD}(t) = 6Dt \tag{4}$$

where D is the diffusion coefficient, and MSD is the value of the mean squared displacement at a particular time t within the diffusive regime. In the simulation times considered, both water and OH^- ions reach the diffusive regime for most systems (long time MSD slope $\approx$ 1), allowing us to calculate their diffusion coefficient from eq 4. The calculated slope in these systems ranges from 0.85 to 0.95 for the hydroxide ions.

We employ the Onsager framework to characterize the dynamic correlation that arises from ion−ion and ion−solvent interactions. The Onsager coefficients[42] can be determined directly from simulations using eq 5 below.

$$L^{ij} = \frac{1}{6k_B TV}\lim_{t\to\infty}\frac{d}{dt}\left\langle \sum_{\alpha}[r_i^{\alpha}(t) - r_i^{\alpha}(0)]\cdot\sum_{\beta}[r_j^{\beta}(t) - r_j^{\beta}(0)]\right\rangle \tag{5}$$

The transport coefficient L^{ij} calculates the degree of correlation between the motion of species i and j. α, β are the specific ions of species i or j. $r_i^{\alpha}(t)$ is the position of anion α at time t. V is the volume of the system, k_B is the Boltzmann constant, and T is the temperature in Kelvin. In our simulations, we use real units where r_i^{α} is in Å, t is in fs, T is in Kelvin, and $k_B = 1.380649 \times 10^{-19}$J/K. L_{ij} is converted to conductivity units (mS/cm) by multiplying by a conversion factor q, $q = 1.60217662 \times 10^{-19}$ e/Coulomb)^2(10^8 Å/cm)(10^{15} fs/s)(10^3 mS/S). L^{ij} values are calculated using a code adopted from Fong et al.[43] and can be interpreted as a measure of correlation between species i and j. When computing L^{ii} to evaluate the ion−ion correlation of ions of species i, the transport coefficient L^{ii} can be divided into two components L^{ii}_{self} where we assess the autocorrelation function of particle α, and $L^{ii}_{distinct}$ where we examine the cross-correlation between two separate particles α, β.

$$L^{ii} = L^{ii}_{self} + L^{ii}_{distinct} \tag{6}$$

L^{ii}_{self} is the Nernst−Einstein contribution arising from ideal, uncorrelated ion motions. In addition to anion−anion correlation and anion−cation correlation, we analyze the correlation between anion and solvent (water) molecules. In total, we have four L^{ij} coefficients to describe the impact of different correlations on hydroxide transport.

RESULTS AND DISCUSSION

Structural Analysis. The microstructure of the polymer, which is directly responsible for the degree of water uptake,

https://doi.org/10.1021/acsapm.4c01827
ACS Appl. Polym. Mater. 2024, 6, 11270−11279

controls the ratio of vehicular vs hopping mechanism in a given system. Thus, it is important to characterize the microstructure of the polymer and map the hydration channels. We do this by employing the cavity energetic sizing algorithm VACUUMMS, as described in the Materials and Methods section, which gives the void size distribution (VSD) for each system. We characterize water channels qualitatively, through visual representations in the form of snapshots of one-nanometer cross-section of the four simulation boxes (Figure 2). Snapshots each taken from one replica of the four corresponding systems show larger more interconnected water channels in PE-A2, followed by PE-A1, PE-P2, and finally PE-P1.

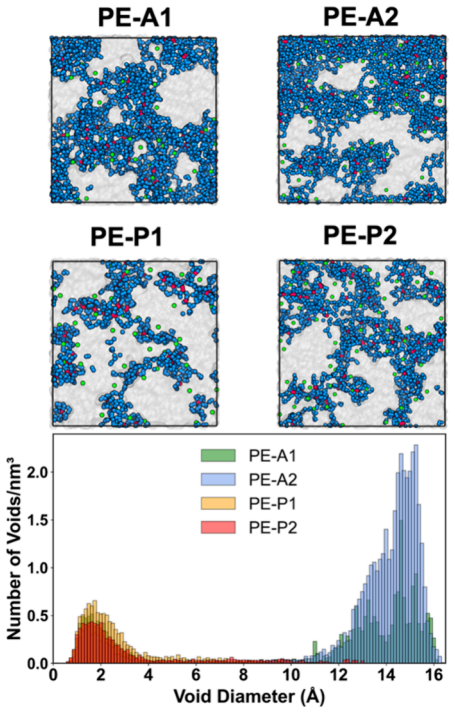

Figure 2. Top: Representative snapshots showing the water channels in the four PE systems, as labeled. Water molecules are in blue, hydroxide ions are in red, nitrogen atoms are in green, and the other polymer groups are transparent and gray. Bottom: Void size distribution showing the number of voids normalized by the box volume as a function of cavity diameter, calculated using VACUUMMS for the four PE polymers, as labeled.

We use the VSD analysis to quantify the size of water channels as described in the Materials and Methods section. VSD distributions of the four systems are also reported in Figure 3. Overall, PE-A1 and PE-A2 have large voids that are >1 nm in diameter, and PE-P1 and PE-P2 have small voids that are ∼0.2 nm in diameter. PE-A2, with the double functional TMA groups (Figure 1) has the largest voids and the broadest void distribution. This is primarily due to steric effects, due to the inability of the bulky TMA group to pack efficiently, allowing greater uptake of water molecules, giving rise to large water channels. On the other end of the spectrum, we have PE-P1 with the smallest void size. Previous studies have shown that polymers with cyclic groups pack compactly, due to pi-pi stacking.[44] This could be why PE-P1 and PE-P2, with the aromatic functional groups, are able to pack more efficiently, resulting in fewer voids and water channels that are smaller in

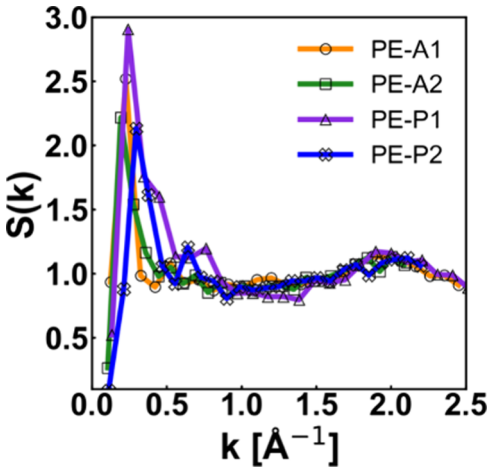

Figure 3. Ion−ion structure factor of the four AEM systems (PE-A1, PE-A2, PE-P1, PE-P2) as labeled.

size compared to PE-A1 and PE-A2, which contain TMA functional groups. Both PE-A1 and PE-A2 have a large void distribution and larger water channels compared to PE-P1 and PE-P2 due to the bulky TMP functional group, leading to a more porous microstructure. The snapshots of the water channels are also in agreement with the void size distribution, with PE-P1 having sparsely connected narrow channels, and PE-A2 has dense water channels (Figure 2). From the snapshots, we see that the water molecules surround the cationic groups along the polymer backbone, and the OH^- ions are associated with the cations as well. Interestingly, the VSD does not seem to be dependent on single vs double chains, but on the functional group instead. TMP PE-A polymers have broader channels, whereas NMP PE-P polymers have narrower channels. We attribute this to the packing of side chains; tightly packed side chains lead to a narrow channel morphology in PE-P1 and PE-P2, and loosely packed chains give rise to larger channels in PE-A1 and PE-A2.

To better correlate polymer microstructure to the water channel width, we compute the structure factor to quantify membrane morphology, specifically, the long-ranged ordering of ion groups. For all four systems, we find a characteristic peak in the structure factor known as the ionomer peak, attributed to the clustering of cationic moieties.[45,46] This suggests microphase separation in the polymers that leads to the formation of ion aggregates, which are responsible for the transport of hydroxyl groups. The position of the ionomer peak corresponds to the characteristic distances between ion clusters, and a shift in peak distance toward lower k values suggests an increase in average separation distance between the clusters. From Figure 3, we see that PE-A1 and PE-A2 have peaks at lower k values, 0.22 $Å^{-1}$ and 0.19 $Å^{-1}$, respectively, compared to PE-P1 and PE-P2 with peaks at 0.29 $Å^{-1}$ and 0.24 $Å^{-1}$, respectively. We compute the characteristic lengths between ionic domains using $d = 2\pi/q$, and we find that these are 2.9, 3.3, 2.6, and 2.2 nm for PE-A1, PE-A2, PE-P1, and PE-P2, respectively. This correlates with trends in void size distribution and water channels from Figure 2, where PE-A1 and PE-A2 have larger domain spacing and cavity size, and PE-P1 and PE-P2 with small domain spacing have smaller cavities. This indicates that TMA headgroups in PE-A1 and PE-A2 lead to ionic clusters that are more spaced out compared to the

https://doi.org/10.1021/acsapm.4c01827
ACS Appl. Polym. Mater. 2024, 6, 11270−11279

NMP headgroups in PE-P1 and PE-P2. The ionic domain sizes in our systems agree well with study of Paren et al.[47]

Next, we calculate the local packing of hydroxide ions near the polymer and water, as well as polymer−polymer packing by computing the radial distribution function (RDF), as described in the Materials and Methods section. Both the distribution of OH^- ions within the polymer matrix and the spatial arrangement of water molecules surrounding the OH^- ions are critical parameters that significantly influence ion transport and thus, conductivity in AEMs. In Figure 4a,b, the H*−H

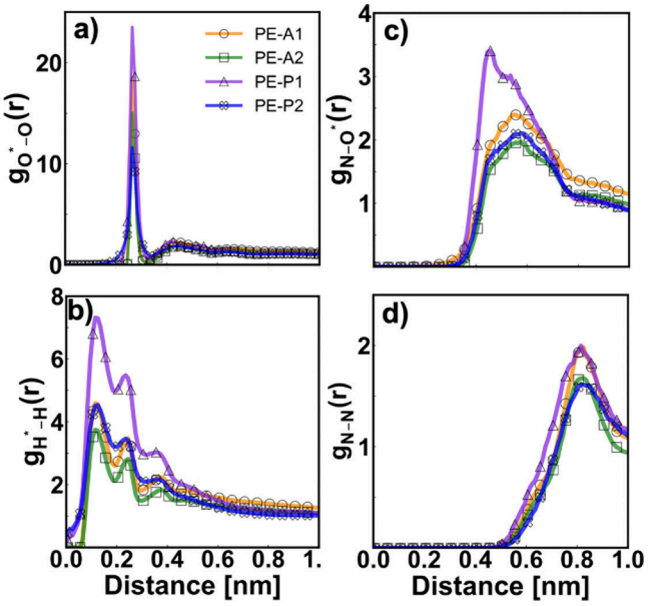

Figure 4. Comparison between the radial distribution functions (RDFs) of PE-A1, PE-A2, PE-P1, PE-P2, as labeled. The RDFs shown are for (a) O*—O (hydroxyl oxygen−water oxygen), (b) H*—H (hydroxyl hydrogen−water hydrogen), (c) N−O* (polymer nitrogen−hydroxyl oxygen), and (d) N−N (polymer nitrogen−polymer nitrogen).

(hydroxide hydrogen−water hydrogen) and the O*−O (hydroxide oxygen−water oxygen) RDF show the arrangement of water around hydroxide ions. We focus on the location (distance) and intensity (magnitude) of the first peak. The first peak in O*−O and the first two peaks in H*−H correspond to the first coordination shell, or the closest water molecules around OH^-. Across all systems, the first peak in O*−O has a high intensity, indicating that the hydroxyl group forms a strong hydrogen bond with the water oxygen, causing both hydroxyl hydrogen and oxygen to pack closely to water molecules. We find that the water−hydroxyl ($g_{O^*-O}(r)$ and $g_{H^*-H}(r)$) and peaks are sharpest in the PE-P1 system (Figure 4a,b), suggesting that the water molecules in PE−P1 are closer and more tightly ordered around the hydroxyl ions than the other PE polymers. On the other hand, PE-A2 shows the smallest $g_{H^*-H}(r)$ and $g_{O^*-O}(r)$ peaks. To quantify the packing of hydroxyl ions around the polymer, we compute the RDF between hydroxyl oxygen and the polymer nitrogen, and this is shown in Figure 4c. The OH^- ions in PE-P1 are packed closer to the cation on the polymer backbone, compared to the other polymers (Figure 4c), and PE-A2 shows the lowest $g_{O^*-N}(r)$ peak. As for the other two systems, (PE-P2 and PE-A1), their water−hydroxyl and polymer−hydroxyl peak intensities are in between the extremes of PE-P1 and PE-A2. These results indicate that, in polymers with a narrow void size distribution (Figure 2), the hydroxyl ions are packed close to both water molecules and cationic groups along the polymer side chain. We also find from $g_{N-N}(r)$ (Figure 4d) the polymer−polymer RDF, that the polymer structures in PE-P1 and PE-A2 are more densely packed, compared to PE-A1 and PE-P2.

To capture the strength of electrostatic interactions between hydroxide ions and cationic functional groups, we compute the potential of mean force (PMF) from the polymer nitrogen−hydroxyl oxygen ($g_{O^*-N}(r)$) radial distribution function. The PMF profiles for the four distinct systems are depicted in Figure 5. The depth of the well correlates with the strength of

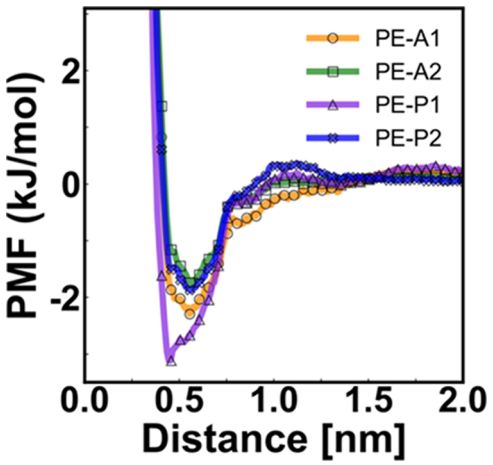

Figure 5. Potential of mean force (PMF) profile as a function of the N−O distance where N is the cationic site, and the O* is the oxygen in the hydroxide ion.

electrostatic interactions. Systems exhibiting reduced well depth, like PE-A2, demonstrate weaker electrostatic interactions between the ammonium and hydroxide anions, resulting in a lower dissociation energy and faster OH^- dynamics. Conversely, systems with a deep PMF well, such as PE-P1, experience stronger interactions and consequently dissociate less readily, leading to slower OH^- dynamics. A reduced well depth in the PMF implies that the cation and anion interaction is weak. In such systems, we expect the hydroxide ion to dissociate readily from the functional group, leading to faster transport and conductivity. We find that both the ion concentration and the nature of the functional groups influence the polymer microstructure. When comparing polymers with the same functional group chemistry but different ion concentrations, such as PE-A1 and PE-A2, we observe larger water channels in PE-A2 as well as lower OH−N interaction strength, primarily due to the increase in water uptake. A similar trend is seen when comparing PE-P1 and PE-P2. When examining the effect of the functional group chemistry while keeping the ion concentration the same, we notice that trimethylammonium-based systems (PE-A1 and PE-A2) allow for higher water uptake and lower OH^-−N^+ interaction strength, compared to methylpiperidinium. This might be due to the compact packing of cyclic groups through pi-pi stacking, resulting in a more efficiently packed system that inhibits higher water uptake.

Details of the membrane microstructure and anion−cation interaction strengths are summarized in Table S2 of the Supporting Information.

https://doi.org/10.1021/acsapm.4c01827
ACS Appl. Polym. Mater. 2024, 6, 11270−11279

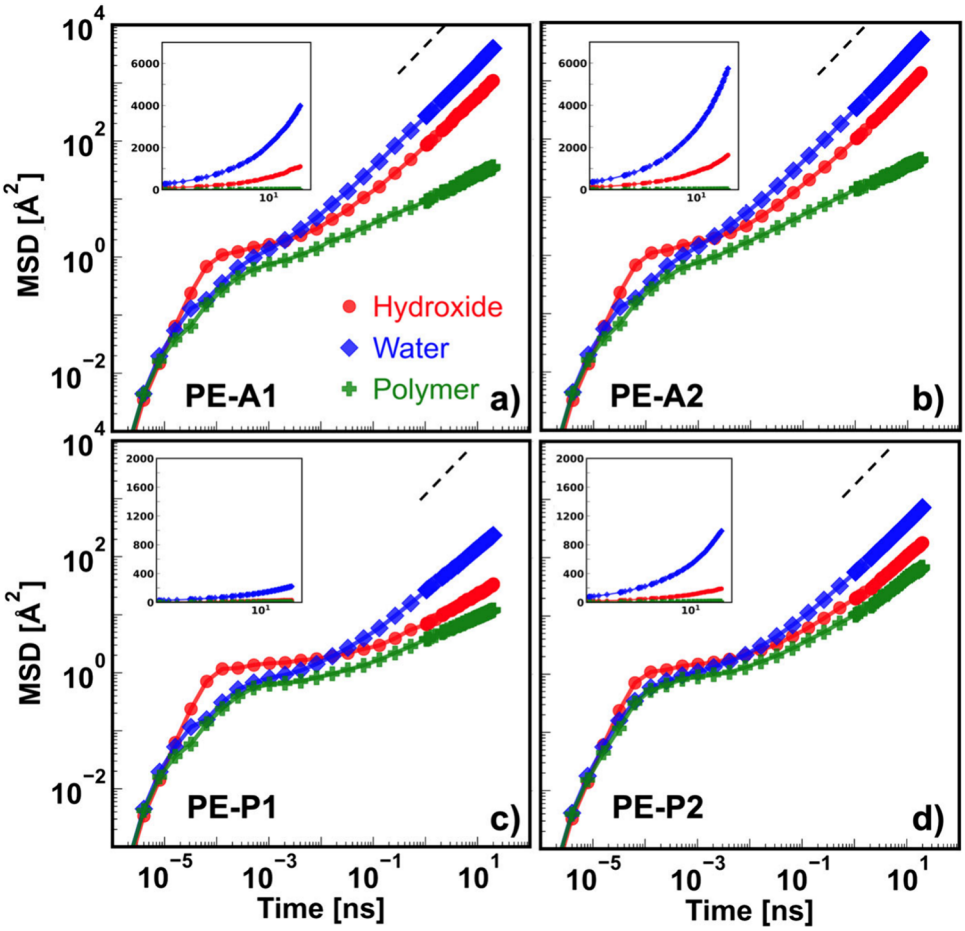

Figure 6. Mean squared displacement (MSD) curves for hydroxide ions, waters, and polymer for a) PE-A1, b) PE-A2, c) PE-P1, and d) PE-P2, as labeled. Insets show log−linear MSD plots, and the dashed line indicates log−log slope of 1.

Transport. To explore the influence of functional group and water channel structure on the transport and dynamics of hydroxide ions, we compute the MSD as described in the Materials and Methods section. To decouple the dynamics of water, polymer and anions, we calculate the MSD of hydroxide ions, water, and polymer separately, as shown in Figure 6. For the four polymers, our analysis reveals that at long times water has the highest mobility, followed by the hydroxide ions, and finally the polymer. At short times, however, the hydroxide ions have a higher mobility than water. At intermediate times, the hydroxide ions exhibit a plateau due to electrostatic interactions with the polymer cations, which arrests their motion. At long times, the hydroxide ions move in unison with water molecules. In this long time regime, vehicular transport of the hydroxide ions facilitated by water molecules dominates. This aligns with prior research, where it has been shown that the diffusion coefficient of hydroxide ions is significantly lower than that of water molecules at high hydration levels.[48] The motion of the polymer chains in the time scale considered has little to no influence on hydroxide ion transport.

Overall, we see that PE-P1 (Figure 6c) and PE-P2 (Figure 6d), with single and double *N*-methylpiperidinium (NMP) groups, respectively, have low hydroxide MSDs compared to PE-A1 (Figure 6a) and PE-A2 (Figure 6b), which contain trimethylammonium groups. The hydroxide ions in the PE-P1 system have not reached the diffusive regime (Figure 6c). We also see that in PE-P1 and PE-P2, the intermediate plateau in the hydroxide MSD is more persistent compared to the plateau in the PE-A1 and PE-A2 systems, signifying that the OH^-−N^+ interactions are stronger in the former, compared to the latter. This is because the hydroxide ions cannot associate closely with the bulky trimethylammonium groups compared to the *N*-methylpiperidinium groups. This is also apparent in the potential of mean force (PMF) curves (Figure 5), with PE-P1 having the lowest minima, signifying a tight association of OH^- with NMP groups. Additionally, it can also be seen that water mobility is higher in the PE-A polymers, compared to the PE-P polymers. It is interesting to note that the PE-P1, with the smallest void size distribution and strongest $g(r)$ peaks shows the lowest hydroxide mobility, and PE-A2 with the broadest void size distribution and the smallest $g(r)$ peaks shows the highest hydroxide mobility. This proves that small voids lead to tighter associations between the hydroxide ions and polymer cations, as well as restricted water motion, which contribute to an overall decrease in hydroxide dynamics.

To quantify the mobility of water molecules and hydroxide ions, we calculate the diffusion coefficient as described in the Materials and Methods section. As expected, water has a higher diffusion coefficient than hydroxide ions in each system. We see a strong correlation between polymer microstructure and hydroxide dynamics, where a more porous microstructure facilitates faster hydroxide transport. We also find that local packing of waters and cations around hydroxide ions is correlated to hydroxide dynamics, as this indicates how effectively the hydroxide ions can dissociate. This underscores the significance of water in facilitating hydroxide transport, as

https://doi.org/10.1021/acsapm.4c01827
ACS Appl. Polym. Mater. 2024, 6, 11270−11279

elucidated in previous sections. For the systems considered, the measured experimental hydroxide conductivity values for PE polymers are 54, 73, 26, and 59 mS/cm for PE-A1, PE-A2, PE-P1, and PE-P2, respectively. We use the Nernst−Einstein approximation to estimate the experimental self-diffusion coefficient from conductivity values and compare it with our simulations. The equation is given by

$$\sigma_{NE} = \frac{e^2}{Vk_BT}(N_+z_+^2\bar{D}_+ + N_-z_-^2\bar{D}_-) \quad (7)$$

where e is the elementary charge, V is the volume of the system, k_B is the Boltzmann constant, T is the temperature, N is the number of ions, z is the charge of the ion, D is the self-diffusion of free ions. The corresponding experimental values of diffusivity are 1.0×10^{-9}, 1.1×10^{-9}, 0.38×10^{-9}, and 0.8×10^{-9} m^2/s for PE-A1, PE-A2, PE-P1, and PE-P2. As seen in Figure 7, our simulation results for diffusivity mirror the experimental trends across the four experimental systems. However, there is an order of magnitude difference in the experimental and simulation values, which has been observed in previous studies as well.[49] For the systems considered here, the origin of the discrepancy is 2-fold. First is our use of the Nernst−Einstein equation, which does not account for ion correlations in conductivity. The second is that our force field does not capture Grotthuss diffusion, which is beyond the scope of our study. However, by comparing the relative deviations in diffusivities, we can comment on which systems would have higher contributions from Grotthuss mechanism. For PE-A1 and PE-A2, the self-diffusion coefficients exhibit deviations of 90% and 88% respectively from experimental values, while for PE-P1 and PE-P2, the deviations are 99% and 98% respectively. Thus, if we assume that all four systems have an equal systematic deviation from experimental values, it is reasonable to conclude that PE-P1 and PE-P2 have greater contributions from Grotthuss transport, compared to PE-A1 and PE-A2. We note that prior studies using reactive simulations have reported that vehicular diffusion contributes to less than 3% of the total hydroxide diffusivity in systems with narrow percolating water channels.[21] This is in line with our results as well; we find that PE-P1 and PE-P2 with narrow void distribution have greater contribution from Grotthuss transport. We note that our systems are run at equilibrium, whereas in the study of Wang et al.,[23] a direct current that splits water molecules to produce OH^- ions is used, and anion conductivity is measured in the presence of an electric field.

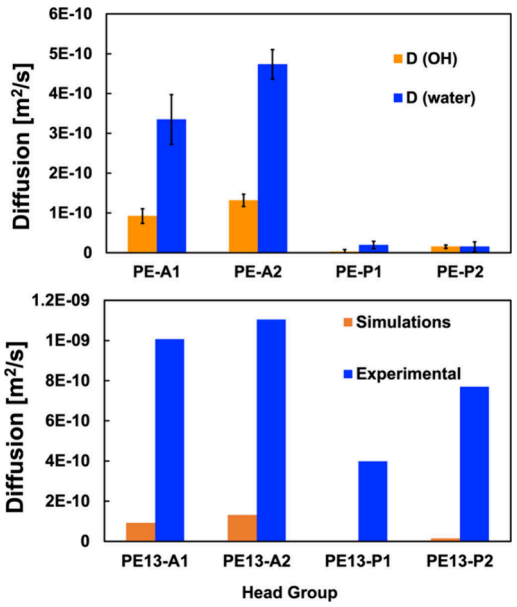

Figure 7. (Top) Self-diffusion coefficient of hydroxide and water calculated from the mean squared diffusion data for the four systems averaged over four replicas. Error bars show one standard deviation. (Bottom) Comparison of the hydroxide self-diffusion coefficient between simulations (estimated from MSD data) and experiments (estimated using conductivity values).

Hydroxide transport in AEMs is often regarded as the uncorrelated movement of ions, where ions are not influenced by other ionic and polar species within the system. The conductivity is derived from the diffusion coefficient under conditions of dilute solutions, where ions are assumed to have no interactions with each other or with counterions and solvent molecules, using the Nernst−Einstein approximation described above (eq 7). Despite its widespread adoption, this approximation overlooks the impact of ion correlation on conductivity values.[50,51] Correlated (concerted) ion motion has a significant effect on ion transport; phenomena such as ion pairing and counterion condensation are important especially at high IEC and low water uptake. However, we do not expect these phenomena to dominate at the water uptake and ion concentrations we consider in this study. To capture correlations in ion motion, we calculate the Onsager coefficients (L^{ij}) described in the Materials and Methods section to examine how dynamic correlations impact the transport of hydroxide ions and thereby affect the overall conductivity. A near zero L^{ij} value corresponds to uncorrelated motion where ions move independently without being influenced by other species. A positive L^{ij} indicates a positive correlation where ions i and j move in the same direction. A negative L^{ij} indicates anticorrelated motions, where ions i and j move in opposite directions. We analyze the correlations impacting the hydroxide transport which include anion−anion correlation L^{--}, anion−cation correlation L^{-+}, and anion-water correlation L^{-w}. As discussed earlier, anion−anion correlation L^{--} is decoupled into a self-term L^{--}_{self} and a distinct term $L^{--}_{distinct}$.

As shown in Figure 8, the L^{--}_{self} is directly proportional to the diffusion coefficient reported in Figure 7 and is equal to the conductivity calculated using the Nernst−Einstein equation. While L^{--}_{self} provides an estimate of the uncorrelated ion motions on the overall transport, correlations could arise from electrostatic, hydrogen bond, or other interactions between different species, which is captured using $L^{--}_{distinct}$. For all four systems, we see that $L^{--}_{distinct}$ has a positive value, suggesting that the hydroxide motions are correlated, or that hydroxide ions are moving in the same direction. However, the magnitude of $L^{--}_{distinct}$ is lower than L^{--}_{self} indicating that the OH^-−OH^- correlations are not large in these systems. Next, we examine the cross correlations between OH^- and the polymer cation (L^{-+}) and water (L^{-w}). In PE-A1 and PE-A2, we observe a negative correlation in L^{-+}, suggesting that the anion and cation move in different directions (Figure 8b). This is because the cations are fixed along the polymer backbone, whose mobility is much lower compared to that of the hydroxide ions and waters (Figure 6), and the hydroxide ions move away from the cations through water clusters leading to an overall anticorrelated cation−anion motion in these systems. In PE-P1 and PE-P2, we find a slightly positive value of L^{-+}, suggesting

https://doi.org/10.1021/acsapm.4c01827
ACS Appl. Polym. Mater. 2024, 6, 11270−11279

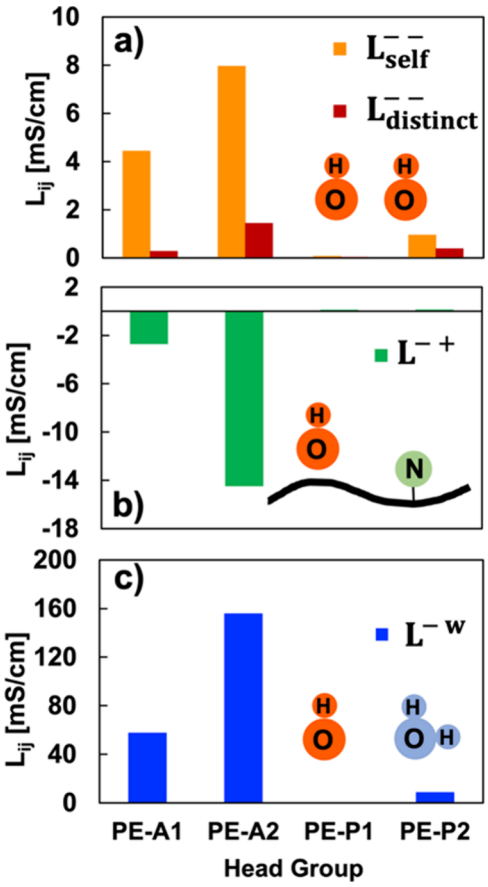

Figure 8. Onsager coefficient L_{ij} characterizing correlations between species i, j in different systems: a) Onsager coefficient L_{ii} between hydroxide ions L^{--}_{self} is the self-part corresponding to self-autocorrelation and $L^{--}_{distinct}$ is the distinct part corresponding to cross-correlation. b) L^{-+} shows the Onsager coefficient for anion−cation correlation. c) L^{-w} the Onsager coefficient for anion-water correlation.

that the hydroxide ions move or hop along the polymer in these systems due to electrostatic effects. Finally, we calculate the OH^--water correlation and find that all systems not only have a positive L^{-w} value, but the magnitude of the L^{-w} coefficient is much higher than the others, suggesting that water facilitates hydroxide transport. Although PE-P1 has the lowest L^{-w} value (0.5 mS/cm), it is still higher than the L^{-+} value (0.13 mS/cm). However, the transport of ions in PE-P1 is likely mediated by both water diffusion as well as ion hopping, as opposed to the other systems which have an overwhelmingly large L^{-w} value. It is also clear that the hydroxide ions move within water clusters, which shields their charge. This is why the $L^{--}_{distinct}$ values in these systems are positive, as there is no electrostatic repulsion between the hydroxide ions shielded by water.

Finally, we perform uniaxial deformation to compute the mechanical properties of these systems, and this is reported in Supporting Information (Figure S1) We find that PE-P2 has the highest toughness, and PE-P1 has the lowest toughness, in accordance with experimental data. We also summarize results from each of our analysis in Table S2 in the Supporting Information.

CONCLUSIONS AND OUTLOOK

In this study, we use atomistic MD simulations to understand how the microstructure of polyethylene-based anion exchange membranes influences hydroxide transport, across four distinct chemistries. The static structure factor reveals distinct ionomer peaks at 1−4 nm^{-1}, signifying microphase separation of ionic domains in the hydrated membranes. We find that a broad void size distribution translates to large, interconnected water channels, which facilitates faster hydroxide diffusion. Radial distribution function and potentials of mean force reveal the local environment around hydroxide ions, and we see that narrow voids lead to tighter packing of water molecules around the hydroxide ions, from which the ions do not dissociate readily. System dynamics are investigated by computing the diffusion coefficients, and we find good agreement with experimental trends. To understand the correlations between ions and water molecules, we calculate the Onsager transport coefficients and establish that the dominant mode of transport in systems with large voids is vehicular (water mediated) diffusion. However, in systems with narrow voids, there is a significant contribution from ion hopping in addition to vehicular transport. Overall, these simulations provide insights into the role of water dynamics and ion correlations on the transport of hydroxide ions. While the trends in hydroxide ion transport between simulations and experiments are consistent, there is discrepancy between the magnitude of simulation and experimental self-diffusion coefficients. This can be attributed to the fact that our classical simulation models do not account for Grotthuss diffusion. Future work will address this issue by approximating reactions using the REACTER force field.[52] This will allow us to directly decouple contributions from reactive and vehicular transport on hydroxide diffusion, particularly in low hydration systems.

ASSOCIATED CONTENT

Data Availability Statement

Data files containing force field parameters and structures can be found here: https://github.com/UFSRG/published-work/tree/main/2024_Polyolefin_AEM

Supporting Information

The Supporting Information is available free of charge at https://pubs.acs.org/doi/10.1021/acsapm.4c01827.

Additional details pertaining to system setup, mechanical property analysis for all four systems, and summary of results (PDF)

AUTHOR INFORMATION

Corresponding Author

Janani Sampath − *Department of Chemical Engineering, University of Florida, Gainesville, Florida 32611, United States;* orcid.org/0000-0001-6005-9096; Email: jsampath@ufl.edu

Authors

Mohammed Al Otmi − *Department of Chemical Engineering, University of Florida, Gainesville, Florida 32611, United States;* orcid.org/0000-0002-9296-440X

Ping Lin − *Department of Chemistry, University of Florida, Gainesville, Florida 32611, United States*

William Schertzer − *School of Materials Science and Engineering, Georgia Institute of Technology, Atlanta, Georgia 30332, United States*

https://doi.org/10.1021/acsapm.4c01827
ACS Appl. Polym. Mater. 2024, 6, 11270−11279

Coray M. Colina − *Department of Chemistry, Department of Materials Science and Engineering, and George and Josephine Butler Polymer Research Laboratory, University of Florida, Gainesville, Florida 32611, United States;* orcid.org/0000-0003-2367-1352

Rampi Ramprasad − *School of Materials Science and Engineering, Georgia Institute of Technology, Atlanta, Georgia 30332, United States;* orcid.org/0000-0003-4630-1565

Complete contact information is available at: https://pubs.acs.org/10.1021/acsapm.4c01827

Notes

The authors declare no competing financial interest.

■ ACKNOWLEDGMENTS

This work was supported as part of UNCAGE-ME, an Energy Frontier Research Center funded by the U.S. Department of Energy, Office of Science, Basic Energy Sciences under Award No. DE-SC0012577. The authors acknowledge University of Florida Research Computing for managing the computational resources that have contributed to the research results reported in this publication. https://www.rc.ufl.edu/. We would also like to acknowledge the reviewers for many helpful comments.

■ REFERENCES

(1) Wee, J.-H. Applications of Proton Exchange Membrane Fuel Cell Systems. *Renew. Sustain. Energy Rev.* **2007**, *11* (8), 1720−1738.
(2) Lu, S.; Pan, J.; Huang, A.; Zhuang, L.; Lu, J. Alkaline Polymer Electrolyte Fuel Cells Completely Free from Noble Metal Catalysts. *Proc. Natl. Acad. Sci. U. S. A.* **2008**, *105* (52), 20611−20614.
(3) Vedarajan, R.; Balaji, R.; Ramya, K. Anion Exchange Membrane Fuel Cell: New Insights and Advancements. *WIREs Energy Environ.* **2023**, DOI: 10.1002/wene.466.
(4) Pan, Z. F.; An, L.; Zhao, T. S.; Tang, Z. K. Advances and Challenges in Alkaline Anion Exchange Membrane Fuel Cells. *Prog. Energy Combust. Sci.* **2018**, *66*, 141−175.
(5) Dong, D.; Wei, X.; Hooper, J. B.; Pan, H.; Bedrov, D. Role of Cationic Groups on Structural and Dynamical Correlations in Hydrated Quaternary Ammonium-Functionalized Poly(p-Phenylene Oxide)-Based Anion Exchange Membranes. *Phys. Chem. Chem. Phys.* **2018**, *20* (29), 19350−19362.
(6) Wang, J.; Zhao, Z.; Gong, F.; Li, S.; Zhang, S. Synthesis of Soluble Poly(Arylene Ether Sulfone) Ionomers with Pendant Quaternary Ammonium Groups for Anion Exchange Membranes. *Macromolecules* **2009**, *42* (22), 8711−8717.
(7) Varcoe, J. R.; Slade, R. C. T. Prospects for Alkaline Anion-Exchange Membranes in Low Temperature Fuel Cells. *Fuel Cells* **2005**, *5* (2), 187−200.
(8) Ran, J.; Wu, L.; He, Y.; Yang, Z.; Wang, Y.; Jiang, C.; Ge, L.; Bakangura, E.; Xu, T. Ion Exchange Membranes: New Developments and Applications. *J. Membr. Sci.* **2017**, *522*, 267−291.
(9) Lin, B.; Qiu, L.; Qiu, B.; Peng, Y.; Yan, F. A Soluble and Conductive Polyfluorene Ionomer with Pendant Imidazolium Groups for Alkaline Fuel Cell Applications. *Macromolecules* **2011**, *44* (24), 9642−9649.
(10) Dang, H.-S.; Weiber, E. A.; Jannasch, P. Poly(Phenylene Oxide) Functionalized with Quaternary Ammonium Groups via Flexible Alkyl Spacers for High-Performance Anion Exchange Membranes. *J. Mater. Chem. A* **2015**, *3* (10), 5280−5284.
(11) Karibayev, M.; Kalybekkyzy, S.; Wang, Y.; Mentbayeva, A. Molecular Modeling in Anion Exchange Membrane Research: A Brief Review of Recent Applications. *Molecules* **2022**, *27* (11), 3574.
(12) Ramírez, S. C.; Paz, R. R. Hydroxide Transport in Anion-Exchange Membranes for Alkaline Fuel Cells. In *New Trends in Ion Exchange Studies*; Karakuş, S., Ed.; InTech, 2018. DOI: DOI: 10.5772/intechopen.77148.
(13) Tomasino, E.; Mukherjee, B.; Ataollahi, N.; Scardi, P. Water Uptake in an Anion Exchange Membrane Based on Polyamine: A First-Principles Study. *J. Phys. Chem. B* **2022**, *126* (38), 7418−7428.
(14) Zelovich, T.; Tuckerman, M. E. OH- and H_3O^+ Diffusion in Model AEMs and PEMs at Low Hydration: Insights from Ab Initio Molecular Dynamics. *Membranes (Basel)* **2021**, *11* (5), 355.
(15) Foglia, F.; Berrod, Q.; Clancy, A. J.; Smith, K.; Gebel, G.; Sakai, V. G.; Appel, M.; Zanotti, J.-M.; Tyagi, M.; Mahmoudi, N.; Miller, T. S.; Varcoe, J. R.; Periasamy, A. P.; Brett, D. J. L.; Shearing, P. R.; Lyonnard, S.; McMillan, P. F. Disentangling Water, Ion and Polymer Dynamics in an Anion Exchange Membrane. *Nat. Mater.* **2022**, *21* (5), 555−563.
(16) Zelovich, T.; Vogt-Maranto, L.; Hickner, M. A.; Paddison, S. J.; Bae, C.; Dekel, D. R.; Tuckerman, M. E. Hydroxide Ion Diffusion in Anion-Exchange Membranes at Low Hydration: Insights from Ab Initio Molecular Dynamics. *Chem. Mater.* **2019**, *31* (15), 5778−5787.
(17) Tuckerman, M. E.; Chandra, A.; Marx, D. A Statistical Mechanical Theory of Proton Transport Kinetics in Hydrogen-Bonded Networks Based on Population Correlation Functions with Applications to Acids and Bases. *J. Chem. Phys.* **2010**, *133* (12), 124108.
(18) Tuckerman, M.; Laasonen, K.; Sprik, M.; Parrinello, M. Ab Initio Molecular Dynamics Simulation of the Solvation and Transport of H3O+ and OH- Ions in Water. *J. Phys. Chem.* **1995**, *99* (16), 5749−5752.
(19) Zhang, W.; van Duin, A. C. T. ReaxFF Reactive Molecular Dynamics Simulation of Functionalized Poly(Phenylene Oxide) Anion Exchange Membrane. *J. Phys. Chem. C* **2015**, *119* (49), 27727−27736.
(20) Chen, C.; Tse, Y.-L. S.; Lindberg, G. E.; Knight, C.; Voth, G. A. Hydroxide Solvation and Transport in Anion Exchange Membranes. *J. Am. Chem. Soc.* **2016**, *138* (3), 991−1000.
(21) Dong, D.; Zhang, W.; van Duin, A. C. T.; Bedrov, D. Grotthuss versus Vehicular Transport of Hydroxide in Anion-Exchange Membranes: Insight from Combined Reactive and Nonreactive Molecular Simulations. *J. Phys. Chem. Lett.* **2018**, *9* (4), 825−829.
(22) Zhang, W.; Dong, D.; Bedrov, D.; van Duin, A. C. T. Hydroxide Transport and Chemical Degradation in Anion Exchange Membranes: A Combined Reactive and Non-Reactive Molecular Simulation Study. *J. Mater. Chem. A* **2019**, *7* (10), 5442−5452.
(23) Wang, T.; Zhang, Y.; Wang, Y.; You, W. Transition-Metal-Free Preparation of Polyethylene-Based Anion Exchange Membranes from Commercial EVA. *Polymer* **2022**, *262*, No. 125439.
(24) Hanwell, M. D.; Curtis, D. E.; Lonie, D. C.; Vandermeersch, T.; Zurek, E.; Hutchison, G. R. Avogadro: An Advanced Semantic Chemical Editor, Visualization, and Analysis Platform. *J. Cheminform.* **2012**, *4* (1), 17.
(25) Bannwarth, C.; Ehlert, S.; Grimme, S. GFN2-XTB-An Accurate and Broadly Parametrized Self-Consistent Tight-Binding Quantum Chemical Method with Multipole Electrostatics and Density-Dependent Dispersion Contributions. *J. Chem. Theory Comput.* **2019**, *15* (3), 1652−1671.
(26) Wang, J.; Wang, W.; Kollman, P. A.; Case, D. A. Automatic Atom Type and Bond Type Perception in Molecular Mechanical Calculations. *J. Mol. Graph. Model.* **2006**, *25* (2), 247−260.
(27) Wang, J.; Wolf, R. M.; Caldwell, J. W.; Kollman, P. A.; Case, D. A. Development and Testing of a General Amber Force Field. *J. Comput. Chem.* **2004**, *25* (9), 1157−1174.
(28) Jakalian, A.; Jack, D. B.; Bayly, C. I. Fast, Efficient Generation of High-Quality Atomic Charges. AM1-BCC Model: II. Parameterization and Validation. *J. Comput. Chem.* **2002**, *23* (16), 1623−1641.
(29) Zhang, X. B.; Liu, Q. L.; Zhu, A. M. An Improved Fully Flexible Fixed-Point Charges Model for Water from Ambient to Supercritical Condition. *Fluid Phase Equilib.* **2007**, *262* (1−2), 210−216.
(30) Fortunato, M. E.; Colina, C. M. Pysimm: A Python Package for Simulation of Molecular Systems. *SoftwareX* **2017**, *6*, 7−12.

(31) Martínez, L.; Andrade, R.; Birgin, E. G.; Martínez, J. M. PACKMOL: A Package for Building Initial Configurations for Molecular Dynamics Simulations. *J. Comput. Chem.* **2009**, *30* (13), 2157−2164.
(32) Zheng, Y.; Ash, U.; Pandey, R. P.; Ozioko, A. G.; Ponce-González, J.; Handl, M.; Weissbach, T.; Varcoe, J. R.; Holdcroft, S.; Liberatore, M. W.; Hiesgen, R.; Dekel, D. R. Water Uptake Study of Anion Exchange Membranes. *Macromolecules* **2018**, *51* (9), 3264−3278.
(33) Pasquini, L.; Di Vona, M. L.; Knauth, P. Effects of Anion Substitution on Hydration, Ionic Conductivity and Mechanical Properties of Anion-Exchange Membranes. *New J. Chem.* **2016**, *40* (4), 3671−3676.
(34) Hagesteijn, K. F. L.; Jiang, S.; Ladewig, B. P. A Review of the Synthesis and Characterization of Anion Exchange Membranes. *J. Mater. Sci.* **2018**, *53* (16), 11131−11150.
(35) Dekel, D. R. Review of Cell Performance in Anion Exchange Membrane Fuel Cells. *J. Power Sources* **2018**, *375*, 158−169.
(36) Larsen, G. S.; Lin, P.; Hart, K. E.; Colina, C. M. Molecular Simulations of PIM-1-like Polymers of Intrinsic Microporosity. *Macromolecules* **2011**, *44* (17), 6944−6951.
(37) Thompson, A. P.; Aktulga, H. M.; Berger, R.; Bolintineanu, D. S.; Brown, W. M.; Crozier, P. S.; in 't Veld, P. J.; Kohlmeyer, A.; Moore, S. G.; Nguyen, T. D.; Shan, R.; Stevens, M. J.; Tranchida, J.; Trott, C.; Plimpton, S. J. LAMMPS - a Flexible Simulation Tool for Particle-Based Materials Modeling at the Atomic, Meso, and Continuum Scales. *Comput. Phys. Commun.* **2022**, *271*, No. 108171.
(38) Willmore, F. T. A Toolkit for the Analysis and Visualization of Free Vol. in Materials. In *Proceedings of the 1st Conference of the Extreme Science and Engineering Discovery Environment on Bridging from the eXtreme to the Campus and beyond - XSEDE '12*; ACM Press: New York, New York, USA, 2012; p 1. DOI: 10.1145/2335755.2335826.
(39) Jiang, Y.; Willmore, F. T.; Sanders, D.; Smith, Z. P.; Ribeiro, C. P.; Doherty, C. M.; Thornton, A.; Hill, A. J.; Freeman, B. D.; Sanchez, I. C. Cavity Size, Sorption and Transport Characteristics of Thermally Rearranged (TR) Polymers. *Polymer* **2011**, *52* (10), 2244−2254.
(40) Willmore, F. T.; Wang, X.; Sanchez, I. C. Free Volume Properties of Model Fluids and Polymers: Shape and Connectivity. *J. Polym. Sci. B Polym. Phys.* **2006**, *44* (9), 1385−1393.
(41) Otmi, M. A.; Willmore, F.; Sampath, J. Structure, Dynamics, and Hydrogen Transport in Amorphous Polymers: An Analysis of the Interplay between Free Volume Element Distribution and Local Segmental Dynamics from Molecular Dynamics Simulations. *Macromolecules* **2023**, *56*, 9042.
(42) Fong, K. D.; Self, J.; McCloskey, B. D.; Persson, K. A. Onsager Transport Coefficients and Transference Numbers in Polyelectrolyte Solutions and Polymerized Ionic Liquids. *Macromolecules* **2020**, *53* (21), 9503−9512.
(43) Fong, K. D.; Self, J.; McCloskey, B. D.; Persson, K. A. Ion Correlations and Their Impact on Transport in Polymer-Based Electrolytes. *Macromolecules* **2021**, *54* (6), 2575−2591.
(44) Hossain, M. D.; Reid, J. C.; Lu, D.; Jia, Z.; Searles, D. J.; Monteiro, M. J. Influence of Constraints within a Cyclic Polymer on Solution Properties. *Biomacromolecules* **2018**, *19* (2), 616−625.
(45) Vandiver, M. A.; Horan, J. L.; Yang, Y.; Tansey, E. T.; Seifert, S.; Liberatore, M. W.; Herring, A. M. Synthesis and Characterization of Perfluoro Quaternary Ammonium Anion Exchange Membranes. *J. Polym. Sci. B Polym. Phys.* **2013**, *51* (24), 1761−1769.
(46) Buggy, N. C.; Du, Y.; Kuo, M.-C.; Ahrens, K. A.; Wilkinson, J. S.; Seifert, S.; Coughlin, E. B.; Herring, A. M. A Polyethylene-Based Triblock Copolymer Anion Exchange Membrane with High Conductivity and Practical Mechanical Properties. *ACS Appl. Polym. Mater.* **2020**, *2* (3), 1294−1303.
(47) Paren, B. A.; Thurston, B. A.; Kanthawar, A.; Neary, W. J.; Kendrick, A.; Maréchal, M.; Kennemur, J. G.; Stevens, M. J.; Frischknecht, A. L.; Winey, K. I. Fluorine-Free Precise Polymer Electrolyte for Efficient Proton Transport: Experiments and Simulations. *Chem. Mater.* **2021**, *33* (15), 6041−6051.
(48) Dubey, V.; Daschakraborty, S. Translational Jump-Diffusion of Hydroxide Ion in Anion Exchange Membrane: Deciphering the Nature of Vehicular Diffusion. *J. Phys. Chem. B* **2022**, *126* (12), 2430−2440.
(49) Webb, M. A.; Jung, Y.; Pesko, D. M.; Savoie, B. M.; Yamamoto, U.; Coates, G. W.; Balsara, N. P.; Wang, Z.-G.; Miller, T. F. Systematic Computational and Experimental Investigation of Lithium-Ion Transport Mechanisms in Polyester-Based Polymer Electrolytes. *ACS Cent. Sci.* **2015**, *1* (4), 198−205.
(50) Marioni, N.; Zhang, Z.; Zofchak, E. S.; Sachar, H. S.; Kadulkar, S.; Freeman, B. D.; Ganesan, V. Impact of Ion-Ion Correlated Motion on Salt Transport in Solvated Ion Exchange Membranes. *ACS Macro Lett.* **2022**, *11* (11), 1258−1264.
(51) France-Lanord, A.; Grossman, J. C. Correlations from Ion Pairing and the Nernst-Einstein Equation. *Phys. Rev. Lett.* **2019**, *122* (13), No. 136001.
(52) Gissinger, J. R.; Jensen, B. D.; Wise, K. E. REACTER: A Heuristic Method for Reactive Molecular Dynamics. *Macromolecules* **2020**, *53* (22), 9953−9961.